Available online at www.sciencedirect.com
SCIENCE DIRECT®
Journal of Organometallic Chemistry 689 (2004) 493–501
Journal of Organometallic Chemistry
www.elsevier.com/locate/jorganchem

The hydrogenphosphate complex of (1,5-cyclooctadiene)iridium(I), $\{[Bu_4N][(1,5\text{-COD})Ir \cdot HPO_4]\}_n$: synthesis, spectroscopic characterization, and ES-MS of a new, preferred precursor to HPO_4^{2-} and Bu_4N^+ stabilized $Ir(0)_n$ nanoclusters

Saim Özkar [a,*], Richard G. Finke [b,*]

[a] Middle East Technical University, Department of Chemistry, 06531 Ankara, Turkey
[b] Department of Chemistry, Colorado State University, Fort Collins, CO 80523, USA

Received 27 July 2003; accepted 30 October 2003

Abstract

The synthesis and characterization of a previously unknown, rare organometallic–phosphate complex, $\{[Bu_4N][(1,5\text{-COD})Ir \cdot HPO_4]\}_n$ (**1**), is described. Characterization of **1** was accomplished by elemental analysis, electrospray mass spectrometry (ES-MS), and ^1H and ^{13}C NMR which established the symmetry of the product as at least C_2 or C_s. The ES-MS reveals an interesting, Ir(I) to Ir(III) oxidative process with intense peaks displaying the $^{191}Ir/^{193}Ir$ isotopic distribution patterns expected for the fragments $[(1,5\text{-COD})Ir^{III}(HPO_4)_2]^-$, $[(C_8H_{11})_2(Ir^{III})_2(PO_4)(HPO_4)(H_2O)]^-$, and $[(C_8H_{11})_2(Ir^{III})_2(PO_4)(HPO_4)(H_2O)_2]^-$. These fragments, in turn, provide evidence for a structure with two HPO_4^{2-} groups attached to a single Ir, for example ring structures (of at least such C_2 or C_s symmetry) such as $\{[Bu_4N][(1,5\text{-COD})Ir \cdot HPO_4]\}_2$. Complex **1** is significant since it is known to be the preferred, compositionally precise precursor to the prototype example of a recently discovered class of novel, HPO_4^{2-} and Bu_4N^+ stabilized nanoclusters, $(Bu_4N)_{2n}^{2n+}[Ir(0)_n \cdot (HPO_4)_n]^{2n-}$. Such nanoclusters are being extended, via their analogous hydrogenphosphate-organometallic precursors $(1,5\text{-COD})M^{+\text{ or }2+}/HPO_4^{2-}$ (M = Rh(I), Ru(II), Pt(II)) to their corresponding, catalytically active $[M(0)_n \cdot (HPO_4)_n]^{2n-}$ nanoclusters.

Keywords: Hydrogenphosphate–organometallic complexes; Synthesis and characterization; Electrospray mass spectrometry of organometallics; Discrete precursors to phosphate-stabilized nanocluster catalysts

1. Introduction

Recently, we reported that the previously unknown complex $\{[Bu_4N][(1,5\text{-COD})Ir \cdot HPO_4]\}_n$ (**1**) served as the *preferred* precursor under H_2 reduction conditions to novel HPO_4^{2-}- and Bu_4N^+-stabilized Ir(0) nanoclusters [1]. The significance of **1** is several fold: (i) Phosphate–*organometallic* complexes are little known even though inorganic metal–phosphate complexes are well precedented [2–11]; hence, **1** is of fundamental interest to organometallic chemistry. (ii) Phosphate is an O-donor ligand and, therefore, is part of a larger literature of O-donor organometallic complexes of, for example, ligands such as $P_2W_{15}Nb_3O_{62}^{9-}$ or $Nb_2W_4O_{19}^{4-}$ polyoxoanions, $P_3O_9^{3-}$, $[P(O)(OR)_2]_3$, $C(Ph_2PO)_3^-$, R_3SiO^-, or simple RO^- (see elsewhere for an extensive list of lead references to these and other O-donor ligands [12]). (iii) Complex **1** is significant as the prototype of a wider class of hydrogenphosphate–organometallic complexes which serve as preferred precursors [1] to transition metal(0) nanoclusters stabilized by the previously unknown – but cheap, robust and recently shown to be quite effective – anionic stabilizer, HPO_4^{2-} [1].

* Corresponding authors. Tel.: +1-970-491-2541; fax: +1-970-491-1801 (R. Finke), Fax: +90-312-210-1280 (S. Özkar).
E-mail addresses: sozkar@metu.edu.tr (S. Özkar), rfinke@lamar.colostate.edu (R.G. Finke).

0022-328X/$ - see front matter © 2003 Elsevier B.V. All rights reserved.
doi:10.1016/j.jorganchem.2003.10.038

Despite the importance of **1** and the other (1,5-COD)M^+ or analogous organometallic complexes of HPO_4^{2-} that are expected to follow this work, only preliminary details of the synthesis and characterization of **1** have been reported [1]. Missing until now are: a more complete analysis and discussion of the spectroscopic and other physical properties of **1** (e.g., its O_2 sensitivity and its thermal analysis/stability), evidence for the molecular formula (i.e., the value of *n*), a discussion of the interesting electrospray mass spectrometry (ES-MS) of **1**, or any idea of the probable structure of **1**. Hence, the full details of the synthesis and characterization of the previously unknown complex, $\{[Bu_4N][(1,5\text{-COD})Ir \cdot HPO_4]\}_n$ (**1**), are presented herein.

2. Results and discussion

2.1. Geometry restrictions of HPO_4^{2-} as a chelating ligand leading to predicted metal-to-ligand stoichiometries and possible structures

It turns out to be quite useful to begin by considering whether or not HPO_4^{2-} will prefer to be a monodentate ligand to the d^8 $Ir^I(1,5\text{-COD})^+$, with its strong preference for square planarity, or if HPO_4^{2-} prefers to be, or even *can be*, a bidentate ligand to $Ir^I(1,5\text{-COD})^+$. Alternatively, HPO_4^{2-} is well-known to serve as a bridging ligand between two metal centers [2]. Yet another, although less likely, possibility is that HPO_4^{2-} could serve as a tridentate ligand to $Ir^I(1,5\text{-COD})^+$, analogous to the five coordinate, tridentate $P_3O_9^{3-}$, in the complex $[(1,5\text{-COD})Ir \cdot P_3O_9]^{2-}$ [13], tridentate $Nb_2W_4O_{19}^{4-}$ in the crystallographically characterized complex $[(1,5\text{-COD})Ir \cdot Nb_2W_4O_{19}]^{3-}$ [13], or tridentate $P_2W_{15}Nb_3O_{62}^{9-}$ polyoxoanion in the ^{17}O and other NMR characterized complex $[(1,5\text{-COD})Ir \cdot P_2W_{15}Nb_3O_{62}]^{8-}$ [12].

A bit of reflection reveals that a key is the O–O span in the tridentate chelating ligands listed above (e.g., 2.8–3.3 Å in $[(1,5\text{-COD})Ir \cdot Nb_2W_4O_{19}]^{3-}$ and $[(1,5\text{-COD})Ir \cdot P_3O_9]^{2-}$) vs the O–O span that is possible in HPO_4^{2-}, 2.5 Å, Scheme 1, from the X-ray diffraction structure of HPO_4^{2-} [14]. That is, an O–O distance in the range of 2.8–3.3 Å is needed to successfully span the two *cis* coordination sites in $Ir^I(1,5\text{-COD})^+$. The key point made apparent by Scheme 1, then, is that HPO_4^{2-} *cannot* span adjacent coordination sites in undistorted, square planar $Ir^I(1,5\text{-COD})^+$, Scheme 1, part B. This in turn means that *monodentate* HPO_4^{2-} coordination (with a solvent at the other coordination site, structure I), a bridging structure (structure II), higher ring structures ($\{[Bu_4N][(1,5\text{-COD})Ir \cdot HPO_4]\}_n$, $n \geqslant 3$; not shown), or conceivably oligomeric structures (not shown) are what one predicts, for **1** as shown in Scheme 1, part B.

2.2. ^{31}P NMR titration of HPO_4^{2-} with $[Ir^I(1,5\text{-COD})(CH_3CN)_2]^+$

The literature teaches the value of up-front titrations ("Job plots" or related titrations) to determine the preferred stoichiometries for organometallic cations plus *polyanions* under the specific solvent, temperature and other conditions employed for the synthesis. Non 1:1 complexes are common, for example the $\geqslant$ 2:1

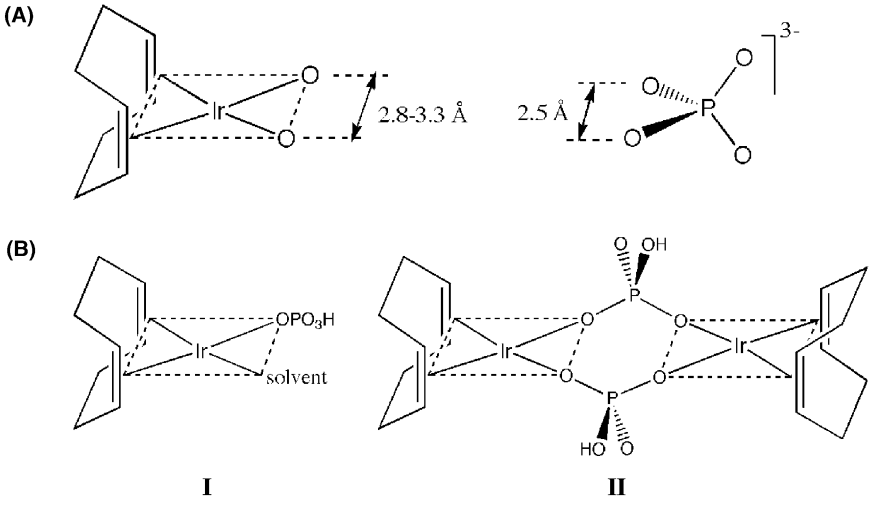

Scheme 1. (A) Crystallographically established O–O distances in $Ir^I(1,5\text{-COD})^+$ complexes with chelating O-donor ligands vs the O–O span possible in hydrogenphosphate. The O–O distances of 2.8 and 3.3 Å are taken from the structures of $[(1,5\text{-COD})Ir \cdot Nb_2W_4O_{19}]^{3-}$ and $[(1,5\text{-COD})Ir \cdot P_3O_9]^{2-}$, respectively [13]. (B) Two possible $Ir(COD)^+$ plus HPO_4^{2-} compositions and structures. Structure II shows one of two isomers; the second isomer (not shown) has the OH groups on P arranged in a *trans* relationship. Not shown are higher ring structures ($n \geqslant 3$), nor conceivable $[-HPO_4 \cdot (1,5\text{-COD})Ir(solvent)-]_n$, and related oligomeric structures; the latter are not shown since they will prove inconsistent with our observed analytical and spectroscopic data. Also conceivable, but not shown, are structures where a face-to-face arrangement of square-planar Ir(I) centers is held together by bridging phosphate ligands.

complexes between $M(NCCH_3)_x^{2+}$ (M = Ni(II), Cu(II), Zn(II) and Cu(I)) and $P_2W_{15}Nb_3O_{62}^{9-}$ [15]. Hence, we began the present work with a ^{31}P NMR titration to determine whether or not a 1:1 HPO_4^{2-} to $Ir^I(1,5\text{-COD})^+$ stoichiometry is preferred at least kinetically if not thermodynamically. The needed titration, Fig. 1, was accomplished by adding 0.20 mL acetonitrile-d_3 solution of 20 μmol $[Ir^I(1,5\text{-COD})(CH_3CN)_2]^+$ to 0.30 mL acetonitrile-d_3 solution of 10, 15, 20, 25, and 30 μmol $[Bu_4N]_2HPO_4$ in separate NMR tubes (the latter prepared in situ from the commercially available $[Bu_4N]HPO_4$ plus Bu_4NOH, followed by storage over 5 Å molecular sieves for 5 h to remove the 1 eq. of H_2O which is generated). As the amount of $[Bu_4N]_2HPO_4$ increases, the relative intensity of the new ^{31}P NMR signal at 14.6 ppm increases linearly up to a 1:1 breakpoint, (Fig. 1) after which it remains constant while the ^{31}P NMR signal of the uncoordinated, free HPO_4^{2-} ion at 5.6 ppm grows in. The preferred 1:1 stoichiometry indicated in Fig. 1 was employed in the subsequent synthetic work.

The order of addition is also important as expected: the opposite order of addition, that is, adding an acetonitrile-d_3 solution of $[Bu_4N]_2HPO_4$ to an acetonitrile-d_3 solution of $[Ir^I(1,5\text{-COD})(CH_3CN)_2]^+$, produced yellow insoluble precipitates, almost surely due to complexes of general formula $\{[Ir^I(1,5\text{-COD})(CH_3CN)_x]_y[HPO_4]_1\}^{2-y}$ where $y > 1$. These complexes did, however, redissolve to yield the same 1:1 complex (by ^1H NMR) once the ratio of $[Bu_4N]_2HPO_4$ to $[Ir^I(1,5\text{-COD})(CH_3CN)_2]^+$ approached 1:1.

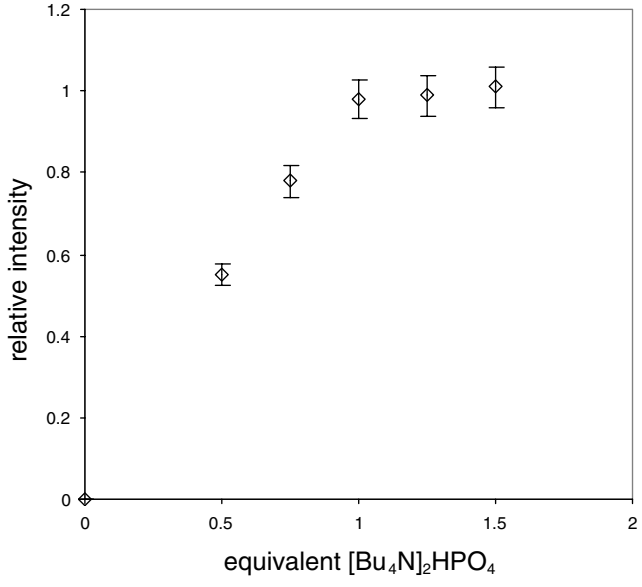

Fig. 1. The ^{31}P NMR titration of $[Ir^I(1,5\text{-COD})(CH_3CN)_2]BF_4$ with $[Bu_4N]HPO_4$. The relative intensity of ^{31}P NMR signal at 14.6 ppm vs the equivalent $[Bu_4N]_2HPO_4$ reveals a breakpoint at a 1:1 stoichiometry.

2.3. Synthesis of $\{[Bu_4N][(1,5\text{-COD})Ir\cdot HPO_4]\}_n$ (1)

Yellow, microcrystalline, analytically pure $\{[Bu_4N][(1,5\text{-COD})Ir\cdot HPO_4]\}_n$ (**1**) in 53% isolated yield was produced by the reaction of 1,5-cyclooctadienebis(acetonitrile)iridium(I) tetrafluoroborate, $[(1,5\text{-COD})Ir(NCCH_3)_2]BF_4$, plus in situ generated tetrabutylammonium monohydrogenphosphate, $[Bu_4N]_2HPO_4$, in acetonitrile according to Eq. (1). Work-up of the reaction consisted of removal of the solvent, trituration using acetonitrile/diethyl ether followed by EtOAc washing to remove any remaining $Bu_4N^+BF_4^-$. The EtOAc washing step is needed, as $Bu_4N^+BF_4^-$ is highly soluble in EtOAc and, without this step, a too-high CHN analysis results due to contamination by residual $Bu_4N^+BF_4^-$. Noteworthy is that the elemental analysis reveals that the 1 eq. of solvent required in possible structures such as I, Scheme 1, or conceivable oligomeric structures, $[-HPO_4\cdot(1,5\text{-COD})Ir(solvent)-]_n$, is *not* present. The ^1H NMR confirms the lack of any coordinated solvent – that is, structure I (Scheme 1, part B) and other such structures requiring a coordinated solvent can be ruled out:

$$\begin{aligned}&\left[(1,5\text{-COD})Ir(NCCH_3)_2\right]BF_4 + [Bu_4N]_2HPO_4\\ &\xrightarrow[CH_3CN]{} \frac{1}{n}\{[Bu_4N][(1,5\text{-COD})Ir\cdot HPO_4]\}_n\\ &\quad + [Bu_4N]BF_4 + 2CH_3CN \qquad (1)\end{aligned}$$

2.4. Characterization of $\{[Bu_4N][(1,5\text{-COD})Ir\cdot HPO_4]\}_n$ (1)

2.4.1. ^1H NMR and ^{13}C NMR

The single ^{31}P NMR peak at 14.59 ppm in acetonitrile-d_3 and the ^1H NMR, vide infra, establish the homogeneity and purity of the complex; the elemental analysis (detailed in Section 3) unequivocally establishes the empirical formula as $\{[Bu_4N][(1,5\text{-COD})Ir\cdot HPO_4]\}_n$ (**1**). The ^1H NMR of **1** in acetonitrile-d_3 of the cyclooctadiene ligand establishes the symmetry of the complex in solution as at least C_2 or C_s by displaying two multiplets for the olefinic protons at 3.48 and 3.30 ppm, two multiplets for the exo hydrogen at 2.31 and 2.18 ppm, and a composite multiplet at 1.25 ppm for the endo CH_2 protons. In addition to the expected four signals for the *n*-butyl groups, the ^1H NMR shows a broad signal centered at 2.26 ppm, which disappears immediately upon addition of a drop of D_2O; hence, this resonance is assigned to the Ir-OPO_3H hydroxyl group. The simple salts $[Bu_4N]H_2PO_4$ and $[Bu_4N]_2HPO_4$ give broad hydroxyl signals at 9.3 and 5.4 ppm, respectively, in their ^1H NMR spectra in acetonitrile-d_3, and under otherwise similar conditions; hence, it appears the presence of the $(1,5\text{-COD})Ir^+$ has a substantial effect on the chemical shift of the $HOPO_3^{2-}$ proton as one might

expect. The $^{13}C\{^1H\}$ NMR spectrum of **1**, also in acetonitrile-d_3, confirms the at least C_2 or C_s symmetry of the complex in solution by exhibiting two signals at 54.71 and 54.54 ppm for the olefinic carbon and two signals at 32.80 and 32.60 ppm for the methylene carbons of the 1,5-COD ligand (along with the four signals expected for the $[Bu_4N]^+$ butyl groups; see Section 3). In short, the elemental analysis and spectroscopic data are definitive in establishing the purity and empirical formula of **1** as $\{[Bu_4N][(1,5\text{-COD})Ir\cdot HPO_4]\}_n$. The data also require a *ring* structure of at least C_2 or C_s symmetry.

2.4.2. Mass spectrometry data

The ES-MS spectrum of the complex **1** proved the most successful of the four MS methods tried (ES-MS, EI-MS, FAB-MS [1] and MALDI-TOF MS [1]), exhibiting one pair of 491, 493 m/z peaks with the characteristic isotopic distribution pattern for one iridium isotope within these peaks (37.3% ^{191}Ir; 62.7% ^{193}Ir). Confirming the $\{(C_8H_{14}IrP_2O_8)_n\}^{n-}$ composition of this $m/n\cdot z$ peak is the essentially exact match between the experimentally recorded and the simulated mass spectra for this composition, Fig. 2. The lack of higher peaks that are multiples of 491/493 (e.g., no 982/986 peaks are seen) is consistent with the assignment of these peaks to the anionic fragment of Ir(III) containing *two* HPO_4^{2-} groups, $[(1,5\text{- COD})Ir^{III}(HPO_4)_2]^-$. This fragment, while not as simple to interpret as a parent ion, is nevertheless suggestive evidence [2] for a structure with two HPO_4^{2-} groups attached to a single Ir, for example composition and structure II in Scheme 1, $\{[(1,5\text{-COD})Ir\cdot HPO_4]_2\}^{2-}$ or, conceivably, other *solvent-free* ring structures, $\{[(1,5\text{-COD})Ir\cdot HPO_4]_n\}^{n-}$. The ES-MS spectrum of the complex **1** provides further evidence for such structures: a group of major peaks at $m/z = 787$, 787, 789, 790, 791, 792 show the characteristic isotopic distribution pattern for two iridium isotopes [3] within these six peaks, peaks which match a simulated $[(C_8H_{11})_2(Ir^{III})_2(PO_4)(HPO_4)]^-$ fragment nearly exactly, Fig. 3. Note that the iridium atoms in this fragment again have the formal oxidation state Ir(III), with each C_8H_{12}-cylcooctadiene ligand losing one proton to form a C_8H_{11}-allyl moiety. The negative ion ES-MS spectrum of **1** exhibits two groups of peaks at $m/z = 805$, 806, 807, 808, 809, 810, and 823, 824, 825, 826, 827, 828 with the same isotopic distribution pattern within each group as the one given in Fig. 3 characteristic of an Ir_2 fragment; these fragments are attributed to $[(C_8H_{11})_2(Ir^{III})_2(PO_4)(HPO_4)(H_2O)]^-$, and its one additional water adduct $[(C_8H_{11})_2(Ir^{III})_2(PO_4)(HPO_4)(H_2O)_2]^-$, respectively. Taken together, the ES-MS results plus the analytical data (i.e., the lack of any coordinated solvent) support the formulation $\{[(1,5\text{-COD})Ir\cdot HPO_4]_n\}^{n-}$ (**1**) where $n \geqslant 2$.

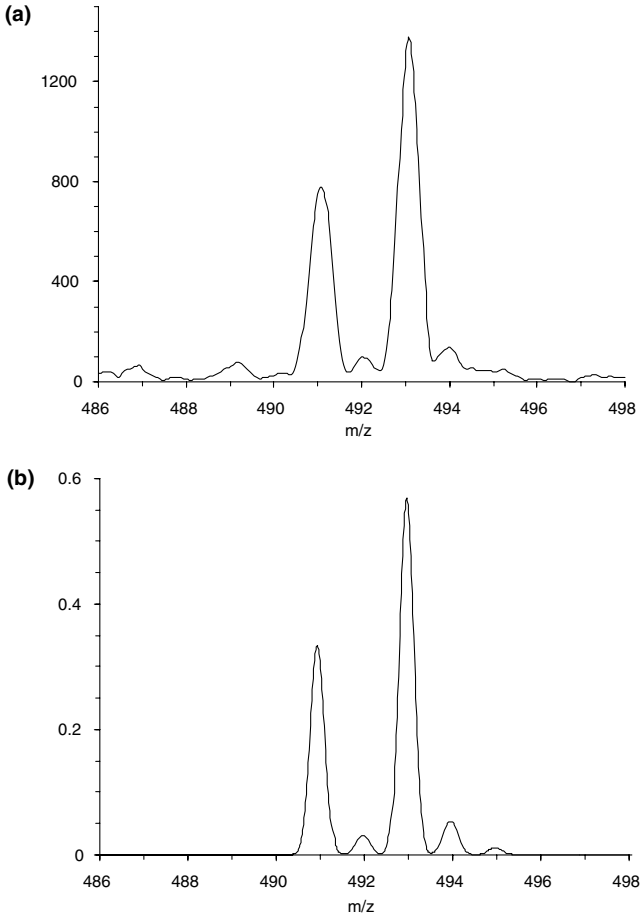

Fig. 2. (a) Experimentally recorded negative ion ES-MS spectrum of the complex $\{[Bu_4N][(1,5\text{-COD})Ir\cdot HPO_4]\}_n$ (**1**) revealing a pair of 491, 493 m/z peaks with the characteristic isotopic distribution pattern for one iridium isotope (37.3% ^{191}Ir; 62.7% ^{193}Ir). (b) Simulated spectrum for the $[(1,5\text{-COD})Ir^{III}(HPO_4)_2]^-$ fragment; note the excellent match of the (a, experimental) and (b, simulated) spectra.

The ES-MS process involving oxidation of Ir(I) to Ir(III) + $2e^-$ is noteworthy: a SciFinder search of the ES-MS literature of organometallic complexes found no prior example of such an oxidation of a transition metal complex under ES-MS conditions. A reasonable explanation of the oxidative ES-MS process is apparent, however. In the Coulomb explosion process within the negative ion ES-MS [16,17], oxidation can plausibly occur by the positively charged electrode plates that can

[1] None of EI, FAB or MALDI-TOF MS exhibited a parent peak. Positive ion FAB shows peaks for clustered products: at $m/z = 1062.0$, $[(COD)_4Ir_3(H_2O)_2H]^+$; 937.2, $[(COD)_3Ir_3(H_2O)_2]^+$; 919.4, $[(COD)_3Ir_3(H_2O)]^+$; 443.2, $[(COD)_2Ir(H_2O)O]^+$. Positive ion ES-MS displays a $[Bu_4N]^+$ peak at $m/z = 242.3$, along with an unidentified peak at $m/z = 888.3$ that has an isotope distribution pattern of a two iridium atom fragment. Positive ion MALDI-TOF in α-cyanocinammic acid matrix gives a peak at $m/z = 563.6$ attributed to the doubly charged $[Bu_4N][(COD)_2Ir_2(PO_4)_3]^{2+}$ ion.

[2] An alternative interpretation is that the concentrating, clustering process of ES-MS may be inducing bimolecular reactions that cause the observed peaks with two (or more) HPO_4^- groups or Ir atoms.

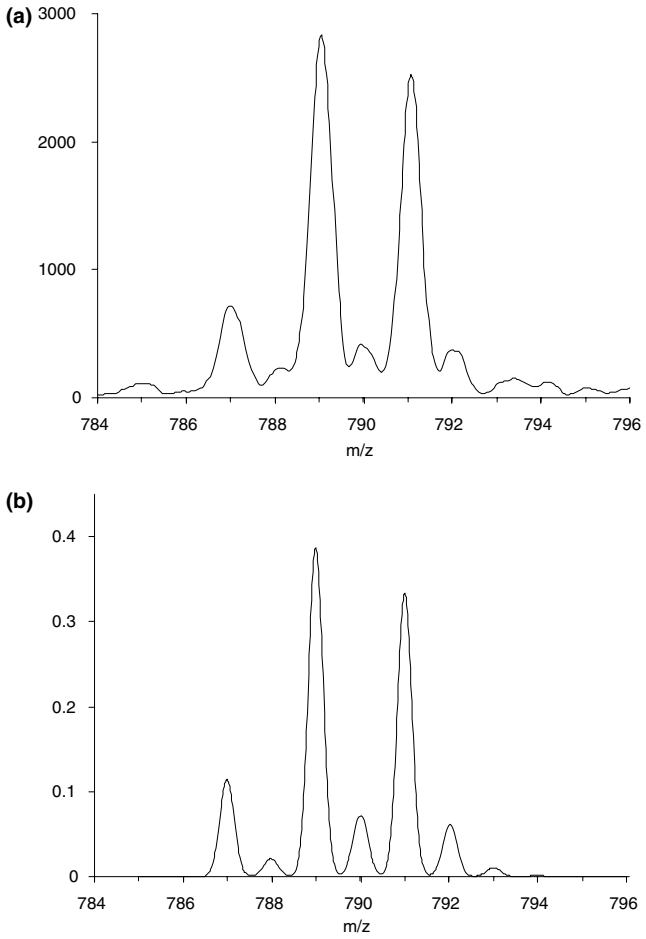

Fig. 3. (a) Experimentally recorded negative ion ES-MS spectrum of the complex $\{[Bu_4N][(1,5\text{-COD})IrHPO_4]\}_n$ (**1**) showing major peaks at $m/z = 787$, 788, 789, 790, 791,792 with the characteristic isotopic distribution pattern for two iridium isotopes (37.3% ^{191}Ir and 62.7% ^{193}Ir). (b) Simulated spectrum for the $[(C_8H_{11})_2(Ir^{III})_2(PO_4)(HPO_4)]^-$ fragment; note the excellent match of the (a, experimental) and (b, simulated) spectra.

have voltages of $\pm$3500 V. [3] (No peak at $m/z = 301$ is seen for the hypothetical, expected to be unstable, "[(1,5-COD)Ir]$^-$" fragment that would have to be produced *if* the electrodes of the ES-MS apparatus are not the oxidant.) A valuable insight from these studies is that ES-MS is not a particularly "soft" [18,19], non-invasive analysis method for at least organometallics with relatively weak, monodentate ligands and bonds such as Ir(I)–OPO_3H.

[3] The fragment $[(1,5\text{-COD})Ir]^+$ is discernible in the positive ion ES-MS spectrum as a pair of 299 and 301 m/z peaks with the characteristic isotopic distribution pattern for one iridium within these peaks. The positive ion ES-MS spectrum also displays the expected Bu_4N^+ peak at $m/z = 242$.

2.5. Attempts at growing single crystals suitable for crystal X-ray crystallography

We delayed publication of this work over a 2 year period while we tried to grow single crystals of **1** suitable for X-ray crystallography. Example methods and solvents from among more than 10 different trials include: gradually cooling solution in acetone/dichloromethane down to −78 °C; vapor phase diffusion of diethyl ether into an acetone or dichloromethane solution of the complex; and slow evaporation of acetone or dichloromethane solutions under reduced pressure conditions at −35 °C. In no case were single crystals, or even microcrystals, observed. Only trituration of an acetonitrile solution of **1** with diethyl ether yielded microcrystals, but no single crystals suitable for X-ray crystallography were ever obtained. Perhaps others will be able to obtain crystals of **1** even though we did not; we welcome such efforts.

2.6. Other physical properties of *1*

Solubility: The complex $\{[Bu_4N][(1,5\text{-COD})Ir \cdot HPO_4]\}_n$ is soluble in polar organic solvents such acetonitrile, dichloromethane, and acetone.

Thermal stability: The complex $\{[Bu_4N][(1,5\text{-COD})Ir \cdot HPO_4]\}_n$ is quite stable as a solid, at temperatures up to ca. 147 °C where it starts to decompose. The TGA shows three regimes of weight loss, but no sharp plateaus so that only an approximate assignment of the weight loss can be made (see Section 3).

O_2 sensitivity: The air-sensitivity of $\{[Bu_4N][(1,5\text{-COD})Ir \cdot HPO_4]\}_n$ was carefully examined by ^{1}H NMR spectroscopy in conjunction with visual observations. Upon exposure to air for 5 min, with shaking to be sure that the solution was well-mixed, the solution failed to show any detectable change in color or in the ^{1}H NMR spectrum. However, after 8 h exposure to air, the yellow clear solution turned brown and the 1,5-COD signals in the ^{1}H NMR spectrum disappeared; the Bu_4N^+ remained constant as expected providing an internal check on the validity of the NMR experiment. In addition to the appearance of weak broad peaks at 5-6 ppm and around 2 ppm, a new broad signal concomitantly grew in at 2.6 ppm that is reminiscent of a hydroxyl proton. The main conclusion is that $\{[Bu_4N][(1,5\text{-COD})Ir \cdot HPO_4]\}_n$ is mildly air (oxygen) sensitive as expected based on the literature of (1,5-COD)Ir(I)$^+$ complexes [12,20].

2.7. Attempted deprotonation of the hydrogenphosphate hydroxyl moiety in *1*

Because the H^+ in $\{[Bu_4N][(1,5\text{-COD})Ir \cdot HPO_4]\}_n$ could be effectively frozen on the ^{1}H NMR timescale in dry, non-protic solvents such as acetonitrile-d_3 (thereby

leading to a C_s symmetry product, consistent with the observed NMR data) we performed an experiment to see if the C_s symmetry restriction could be lifted by the addition of 1 eq. of base. The bottom line of this experiment is that, even after 24 h, 1 eq. of Proton Sponge™ [1,8-bis(dimethylamino)naphthalene] (*aqueous* $pK_a = 12.3$ [21,22]) added to **1** in acetonitrile-d_3 produced *no detectable change* in either the ^1H NMR or in the appearance to the eye of the clear, yellow solution. This is despite the HPO_4^{2-} *aqueous* pK_{a3} of 12.4 [23] being similar to that of Proton Sponge™, and despite the expected lowering by at least 1–2 pK_a units of the HPO_4^{2-} pK_a by coordination to the cationic (1,5-COD)Ir^+ group. Further details are provided in Section 3.

2.8. Summary

In summary, the synthesis, elemental analysis and spectroscopic characterization of the first of a prototype example of a preferred precursor [1] to phosphate- and Bu_4N^+-stabilized $Ir(0)_n$, and by implication other metal$(0)_m$, nanoclusters has been described, $\{[Bu_4N][(1,5\text{-COD})Ir \cdot HPO_4]\}_n$ (**1**). The resultant analytically pure, compositionally characterized material, a rare example of a phosphate-organometallic complex, possesses at least C_2 or C_s symmetry, and most likely has two Ir–OPO_3H bonds by ES-MS evidence; ring structures, such as the $n = 2$ structure II in Scheme 1, are indicated.

The importance of **1** as a precursor to $Ir(0)_n \cdot (HPO_4^{2-})_n$ nanoclusters has recently been described [1]; only the reproducible, *known* 1 Ir: 1 HPO_4^{2-} composition of **1** is crucial to that nanocluster formation reaction, the Ir–OPO_3H bond in **1** being broken and replaced by Ir(0)–Ir(0), and $Ir(0)_n$–OPO_3H bond, in the nanocluster product [1]. Hence, application of the synthetic methods herein promise to be more general and are in progress for the (1,5-COD)$M^{+\text{ or }2+}$/HPO_4^{2-} complexes of M = Rh(I), Ru(II), Pt(II) en route to other, highly desirable, catalytically active nanoclusters [24].

3. Experimental

Materials. All commercially obtained compounds were used as received unless indicated otherwise. Aqueous Bu_4NOH solutions (40% in water, Aldrich, freshly opened) were triturated separately with 0.1 M HCl to methyl red and phenolphthalein end points (i.e., for both amine and total base content) immediately prior to use. $AgBF_4$ (Aldrich) was purified by extraction with diethyl ether followed by evaporation of the extract under vacuum to give a white powder. Deuterated NMR solvents D_2O, CD_3CN, and CD_2Cl_2 (Cambridge Isotope Laboratories) were received in 1 mL glass ampoules which were transferred into the drybox where sample preparation for NMR were performed. Yellow, crystalline iridium solvate complex, [(1,5-COD)$Ir(NCCH_3)_2$]BF_4, was prepared according to the procedure given in the literature for the corresponding hexafluorophosphate salt [13]; the product was identified by ^1H and ^{13}C spectroscopy in dichorometane-d_3 in comparison to the literature spectral data of the hexafluorophosphate salt [13]: ^1H NMR: δ (ppm, rel.TMS) = 4.32 (CH), 2.61 (CH_3), 2.34 (CH_2), 1.86 (CH_2); ^{13}C-NMR: δ (ppm, rel. TMS) = 123.92 (CN), 71.92 (CH), 31.62 (CH_2), 3.86 (CH_3).

3.1. Instrumental methods

High resolution solution NMR spectra were taken on a Varian INOVA-300 instrument (^1H, 300.115; ^{13}C, 75.472; and ^{31}P, 121.489 MHz). IR spectra were taken on a Nicolet 5PC FTIR spectrometer from the KBr pellet. Elemental analyses were done by Atlantic Microlabs and by Galbraith Laboratories, Inc and were performed with air-free handling. TGA was run on a TA Instruments TA 2950 using a platinum pan, purged with helium with 10 °C/min heating rate. ES-MS was done on a fisons VG Quattro-sQ, FAB-MS was done on a Fisons VG Autospec with m-nitrobenzylalcohol as matrix, EI-MS was also done on a Fisons VG Autospec with 70 eV, 8 kV acceleration voltage and O_2 free precautions. Simulations (i.e., as shown in Figs. 2 and 3) were done by using Fisons VG MassLynx or ThermoFinnigan Xcalibur Isotope Viewer software. MALDI-TOF MS was obtained in the Molecular Resources center at Colorado State University, in the Department of Biochemistry, on a Perceptive Biosystem Model Voyager DEPRO using three different matrices: α-cyanocinammic, 2,5-dihydroxybenzoic acid, and azothiothymine.

3.2. Air-free manipulations

Unless otherwise reported all reactions and manipulations were carried out under oxygen- and moisture-free conditions using a Vacuum Atmospheres nitrogen drybox $\leqslant 2$ ppm O_2 as continuously monitored by a Vacuum Atmospheres O_2-level monitor). NMR samples were prepared in the drybox and then the sample tubes were capped with a small rubber septum and taken out of the drybox.

3.3. ^{31}P NMR titrations

3.3.1. Adding $[Ir^I(1,5\text{-COD})(CH_3CN)_2]^+$ to $[Bu_4N]_2$-HPO_4

First, 169.5 mg $TBAH_2PO_4$ (0.5 mmol) was weighed in a 2-dram vial and dissolved in 1.5 mL acetonitrile-d_3 (CD_3CN). Next, 0.5 mL of 1.0 M TBAOH was added with a 1.0 mL gas-tight syringe. The solution was stirred and then left over 5 Å molecular sieves for 5 h to remove

the H_2O formed. After decantation, the volume of the solution was adjusted to 2.0 mL by adding acetonitrile-d_3: $[Bu_4N]_2HPO_4 = 0.200$ mM, or 250 μmol per mL. Aliquots of 40, 60, 80, 100, and 120 μL (10, 15, 20, 25, and 30 μmol $[Bu_4N]_2HPO_4$, respectively) of this solution was transferred into five separate NMR tubes using a 100 μL gas-tight syringe. The volume of the solutions in the NMR tubes was adjusted to 0.30 mL by adding required amount of deuterated acetonitrile (260, 240, 220, 200, and 180 μL, respectively). In a 2-dram glass vial, 56.3 mg (0.12 mmol) $[(COD)Ir(NCCH_3)_2]BF_4$ was weighed and dissolved in 1.2 mL acetonitrile-d_3. The solution contained 0.100 mM $[(COD)Ir(NCCH_3)_2]BF_4$ (or 100 μmol $[(COD)Ir(NCCH_3)_2]BF_4$ per mL). Into each NMR tube a 200 μL aliquot of this solution (20 μmol $[(COD)Ir(NCCH_3)_2]BF_4$) was added with a 250 μL gas-tight syringe. The solutions in the NMR tubes (exactly 0.50 mL) were shaken for 5 min and left standing for $\geqslant 5$ h in the drybox to ensure complete reaction. The ^{31}P NMR spectra were taken under the same instrumental conditions (512 scans for each). As the amount of $[Bu_4N]_2HPO_4$ increased the relative intensity of the new ^{31}P NMR signal at 14.6 ppm increases linearly up to its equivalence point (Fig. 1), then remains constant as the ^{31}P NMR signal for the free HPO_4^{2-} ion at 5.6 ppm grows in.

3.3.2. The opposite order of addition, adding $[Bu_4N]_2HPO_4$ to $[Ir^I(1,5\text{-}COD)(CH_3CN)_2]^+$

First, 200 μL aliquots of the 0.100 mM $[(COD)Ir(NCCH_3)_2]BF_4$ solution in acetonitrile-d_3 (each containing 20 μmol $[(COD)Ir(NCCH_3)_2]BF_4$) were transferred into five NMR tubes using a 250 μL gas-tight syringe). Next, 40, 60, 80, 100, or 120 μL aliquots of 0.200 mM $[Bu_4N]_2HPO_4$ in acetonitrile-d_3 (10, 15, 20, 25, or 30 μmol $[Bu_4N]_2HPO_4$, respectively) were added to the solutions in the NMR tube with a 100 μL gas-tight syringe. The volume of the solutions in the NMR tubes were completed to 0.50 mL by adding required amount of acetonitrile-d_3 (260, 240, 220, 200, and 180 μL, respectively). However, a yellow precipitate was observed in the first three sample tubes upon addition of the $[Bu_4N]_2HPO_4$ solution to the $[(COD)Ir(NCCH_3)_2]BF_4$ solution. Shaking the NMR tube did not dissolve the precipitate completely; some of it remained stuck to the NMR tube walls, insoluble precipitates due, almost surely, to complexes of general formula $y > 1$: $\{[Ir^I(1,5\text{-}COD)(CH_3CN)_x]_y[HPO_4]_1\}^{2-y}$. These precipitates do, however, dissolve with vigorous stirring for longer times.

3.4. Synthesis of $\{[Bu_4N][(1,5\text{-}COD)Ir\cdot HPO_4]\}_n$ (1)

All manipulations were carried out in the drybox. First, 0.183 g (0.540 mmol) of $(Bu_4N)H_2PO_4$ was dissolved in 3 mL CH_3CN in a 100 mL round-bottomed flask, then 0.54 mL (0.54 mmol) of 1M Bu_4NOH aqueous solution was added. The solution was stirred for 3 h and then dried over mol. sieves to remove the water. A solution of 0.254 g (0.540 mmol) $[(1,5\text{-}COD)Ir(NCCH_3)_2]BF_4$ in 3 mL CH_3CN was added to the phosphate solution in the round-bottomed flask and the final solution was stirred for 3 h. The yellow color of the solution did not change. The volume of the solution was reduced by evaporation under vacuum to 2 mL. The dark-yellow solution was added dropwise into 200 mL diethyl ether in a beaker. During this addition yellow microcrystals began to precipitate. The stirring was continued for 10 min after the addition. The yellow microcrystalline solid was collected over a 35 mL medium glass frit by suction filtration, washed with 2×25 mL of diethyl ether *and ethyl acetate* (in which the by-product $Bu_4N^+BF_4^-$ is highly soluble), dried and vacuum for 4 h (0.183g, 0.28 mmol, 53%), and stored in the dry box. m.p.: 147 °C (decomp.). *Anal.* Calc. for $C_{24}H_{49}NO_4PIr$: C, 45.11; H, 7.75; N, 2.19; (O, 10.02; P, 4.85; Ir, 30.08), Found (Atlantic Microlab): C, 45.27; H, 7.64; N, 2.22%. Found (Galbraith Laboratories, Inc.): C, 45.41; H, 7.70; N, 2.23; P, 5.43 ($\pm \geqslant 0.4$); Ir, 32.84 ($\pm > 0.8$). Two different batches were analyzed by Atlantic Labs and Galbraith Laboratories, Inc. The C, H, and N values of both analyses are in excellent agreement with the values calculated for the formula $\{[Bu_4N][(1,5\text{-}COD)Ir\cdot HPO_4]\}_2$. The fact that the CHN calculated and found values are in excellent agreement, and the P:Ir ratio is 1.02, means that pure, 1 P : 1 Ir adduct has been prepared. The correct CHN analysis and 1.02 P:Ir ratio also strongly suggests that the true error bars on the P and Ir analyses are large enough to bring them in agreement with their calculated values. [See footnote 3 elsewhere where, for example, ±3% error bars on (in that example) Ru analyses from selected vendors under certain conditions are detailed [25].]

3.5. Further characterization of $\{[Bu_4N][(1,5\text{-}COD)Ir\cdot HPO_4]\}_n$ (1)

IR (KBr pellet) 3480 (m, br), 2960 (s), 2874 (s), 1474 (s), 1458 (s), 1204 (s), 1186 (s), 1043 (s), 1014 (s) 567 (w) cm^{-1}. ^1H NMR (300 MHz, CD_3CN, 22 °C): δ (ppm, rel. TMS) 3.48 (CH, m, 2), 3.30 (CH, m, 20, 2.31 (exo CH_2, m, 2), 2.18 (exo CH_2, m, 2), 1.25 (endo CH_2, m, 4), 3.10 (N-CH_2, m, 8), 1.62 (CH_2, m, 8), 1.38 (CH_2, m, 8), 0.98 (CH_3, t, 12), 2.26 ($HOPO_3^-$, broad, disappears immediately upon addition of a drop of D_2O into the NMR tube). $^{13}C\{^1H\}$ NMR (75 MHz, CD_3CN, 22 °C): δ (ppm, rel. TMS) 54.707 (=CH), 54.537 (=CH), 32.796 (=CH–CH_2), 32.594 (=CH–CH_2), 59.382 (N–CH_2), 24.441 (CH_2), 20.438 (CH_2), 13.935 (CH_3). $^{31}P\{^1H\}$ NMR (75 MHz, CD_3CN, 22 °C): δ 14.66 (ppm, relative to 85% H_3PO_4 in a concentric glass capillary internally immersed in the same NMR tube). Negative ion ES-MS

spectrum in acetonitrile gives a pair of main (but not base, nor parent) peaks at 491/493 m/z that matches essentially exactly the characteristic isotope distribution for one iridium atom, Fig. 2, peaks assigned to $[(1,5\text{-COD})\text{Ir}(\text{HPO}_4)_2]^-$ as discussed in the main text. The negative ion ES-MS spectrum also exhibits a group of major peaks at $m/z = 787$, 787, 789, 790, 791, 792 with the characteristic isotopic distribution pattern for two iridium isotopes, assigned to $[(\text{C}_8\text{H}_{11})_2(\text{Ir}^{\text{III}})_2(\text{PO}_4)(\text{HPO}_4)]^-$, Fig. 3. Furthermore, two groups of peaks at $m/z = 805$, 806, 807, 808, 809, 810, and 823, 824, 825, 826, 827, 828 with the same isotopic distribution pattern for two Ir atoms are assigned to $[(\text{C}_8\text{H}_{11})_2(\text{Ir}^{\text{III}})_2(\text{PO}_4)(\text{HPO}_4)(\text{H}_2\text{O})]^-$, and its one additional water adduct $[(\text{C}_8\text{H}_{11})_2(\text{Ir}^{\text{III}})_2(\text{PO}_4)(\text{HPO}_4)(\text{H}_2\text{O})_2]^-$, respectively. Positive ion ES-MS in acetonitrile gives a peak at 242.3 m/z assigned to $[\text{Bu}_4\text{N}]^+$ plus an unidentified peak at $m/z = 888.3$ with a two iridium isotope distribution pattern. Positive ion FAB shows peaks for clustered products: at $m/z = 1062.0$, $[(\text{COD})_4\text{Ir}_3(\text{H}_2\text{O})_2\text{H}]^+$; $m/z = 937.2$, $[(\text{COD})_3\text{Ir}_3(\text{H}_2\text{O})_2]^+$; $m/z = 919.4$ $[(\text{COD})_3\text{Ir}_3(\text{H}_2\text{O})]^+$; and $m/z = 443.2$, $[(\text{COD})_2\text{Ir}(\text{H}_2\text{O})\text{O}]^+$. Positive ion MALDI-TOF in α-cyanocinammic acid matrix gives a peak at $m/z = 563.6$ attributed to a doubly charged $[\text{Bu}_4\text{N}][(\text{COD})_2\text{Ir}_2(\text{PO}_4)_3]^{2+}$ ion. TGA of **1** under helium at heating rate of 10 °C/min shows three approximate regimes of weight loss, but no sharp plateaus, so that only an approximate assignment of the weight loss can be made: from ca. 175 °C to 350 °C a total loss of 49.4 wt% is seen. No exact accounting for this thermal weight loss under a helium atmosphere is apparent; for example, loss of COD, Bu_3N, butene and H_2 to a hypothetical IrPO_4 residue predicts a calculated weight loss of 55.0 wt%.

3.6. ^{1}H NMR determination of the O_2 sensitivity of $\{[Bu_4N][(1,5\text{-COD})Ir\cdot HPO_4]\}_n$ (1)

In 2-dram glass vial, 11.5 mg (18 μmol Ir) of $\{[\text{Bu}_4\text{N}][(1,5\text{-COD})\text{Ir}\cdot\text{HPO}_4]\}_2$ was dissolved in 0.5 mL acetonitrile-d_3. The solution was transferred into a NMR sample tube with a disposable polyethylene pipette, then capped with a rubber septum and taken out of the drybox. After having first taken a "zero-time" ^{1}H NMR spectrum, the solution was exposed to air for 5 min, with shaking to ensure good mixing. Neither the yellow color, nor the ^{1}H NMR spectrum, produced any detectable change over 5 min. After 8 h exposure to air, the previously clear yellow solution had turned brown and the 1,5-COD signals in the ^{1}H NMR spectrum had disappeared; the fact that the Bu_4N^+ butyl groups did *not* change shows that the NMR was still functioning and tuned properly. In addition to the appearance of weak, broad peaks at 5-6 ppm and around 2 ppm, a new broad signal concomitantly grew in at 2.6 ppm, attributable to a hydroxyl proton. Overall, this NMR control experiment reveals the expected [12 (see footnote 18); 20], air-sensitivity of $\{[\text{Bu}_4\text{N}][(1,5\text{-COD})\text{Ir}\cdot\text{HPO}_4]\}_n$.

3.7. Attempted deprotonation of the hydrogenphosphate hydroxyl moiety in 1

In a 2-dram glass vial, 11.5 mg (18 μmol Ir) of $\{[\text{Bu}_4\text{N}][(1,5\text{-COD})\text{Ir}\cdot\text{HPO}_4]\}_n$ and 3.8 mg (18 μmol, 1.0 equivalent) Proton Sponge™ [1,8-bis(dimethylamino)naphthalene] were dissolved in 0.5 mL acetonitrile-d_3. The solution was transferred into a NMR sample tube with a disposable polyethylene pipette, capped with a small rubber septum, and removed from the drybox. The first ^{1}H NMR spectrum, taken as soon as possible, was exactly the same as the complex **1** alone, plus the four signals of Proton Sponge™ at 7.48 (CH), 7.44 (CH), 7.05 (CH), and 2.91 (CH_3) ppm. After 24 h there was still no noticeable change in the ^{1}H NMR spectrum of the complex; the clear, yellow solution remained visually unaltered as well.

Note added in proof

Additional scouring of the literature for complexes *related* to organometallic phosphate systems located two important papers by Shapley and co-workers. Those papers describe interesting, crystallographically characterized $\text{H}_2\text{OS}_3(\text{CO})_9(\mu_3\text{-O}_3\text{ER})$ complexes (ER = PR; SO; AsR) which anyone interested in the topic of PO_4^3, SO_4^{2-}, O_3PR^{2-} and related organometallic complexes will wish to consult [26,27].

Acknowledgements

This work was supported by grant DE-FG02-03ER15453 from the Chemical Sciences, Geosciences and Bioscience Division, Office of Basic Energy Sciences, Office of Science, U.S. Department of Energy.

References

[1] S. Özkar, R.G. Finke, Langmuir 19 (2003) 6247.
[2] L. Yin, P. Cheng, S.P. Yan, X.Q. Fu, J. Li, D.Z. Liao, Z.H. Jiang, J. Chem. Soc., Dalton Trans. (2001) 1398.
[3] C. He, V. Gomez, B. Spingler, S.J. Lippard, Inorg. Chem. 39 (2000) 4188.
[4] C. He, S.J. Lippard, J. Am. Chem. Soc. 122 (2000) 184.
[5] J.J. Wilker, S.J. Lippard, Inorg. Chem. 38 (1999) 3569.
[6] T. Tanase, J.W. Yun, S.J. Lippard, Inorg. Chem. 35 (1996) 3585.
[7] S.M. Gorun, S.J. Lippard, Inorg. Chem. 30 (1991) 1625.
[8] M.D. Hopkins, V.M. Miskowski, H.B. Gray, J. Am. Chem. Soc. 112 (1990) 959.
[9] D.R. Cranel, P.C. Ford, J. Am. Chem. Soc. 112 (1990) 6871.
[10] R. El-Mehdawi, F.R. Fronczek, D.M. Roundhill, Inorg. Chem. 25 (1986) 25, 1155.

[11] F.A. Cotton, L.R. Falvello, S. Han, Inorg. Chem. 21 (1982) 1709.
[12] M. Pohl, D.K. Lyon, N. Mizuno, K. Nomiya, R.G. Finke, Inorg. Chem. 34 (1995) 1413 (see footnote 5 therein).
[13] V.W. Day, W.G. Klemperer, D.J. Main, Inorg. Chem. 29 (1990) 2345.
[14] A. Boukhris, C. Lecomte, B. Wyncke, F. Brehat, A. Thalal, J. Phys.: Condens. Matter 6 (1994) 2475.
[15] H. Weiner, Y. Hayashi, R.G. Finke, Inorg. Chem. 38 (1999) 2579.
[16] G.J. Van Berkel, F. Zou, Anal. Chem. 66 (1994) 3408.
[17] G. Zoorob, F.B. Brown, J. Caruso, J. Anal. Atomic Spect. 12 (1997) 517.
[18] K.J. Light-Wahl, D.L. Springer, B.E. Winger, C.G. Edmonds, D.G. Camp II, B.D. Thrll, R.D. Smith, J. Am. Chem. Soc. 115 (1993) 804.
[19] J.B. Fenn, M. Mann, C.K. Meng, S.F. Wong, C.M. Whitehouse, Science 246 (1989) 64.
[20] V.W. Day, W.G. Klemperer, S.P. Lockledge, D.J. Main, J. Am. Chem. Soc. 112 (1990) 2013.
[21] B. Brzezinski, G. Schroeder, E. Grech, Z. Malarski, L. Sobczyk, J. Mol. Struct. 274 (1992) 75.
[22] B. Brzezinski, T. Glowiak, E. Grech, Z. Malarski, L. Sobczyk, J. Chem. Soc., Perkin Trans. 2 (1991) 1643.
[23] N.N. Greenwood, A. Earnshaw, Chemistry of The Elements, Pergamon Press, New York, 1984, p. 598.
[24] R.G. Finke, E. Finney, unpublished results and experiments in progress.
[25] J.A. Widegren, H. Weiner, S.M. Miller, R.G. Finke, J. Organomet. Chem 610 (2000) 112.
[26] R.L. Keiter, D.S. Strickland, S.R. Wilson, J.R. Shapley, J. Am. Chem. Soc. 108 (1986) 3846.
[27] G.R. Frauenhoff, J.-C. Liu, S.R. Wilson, J.R. Shapley, J. Organomet. Chem. 437 (1992) 347.